PAPER

Stacked Rectangular Microstrip Antenna with a Shorting Plate and a Helical Pin for Triple Band Operation in ITS

Takafumi FUJIMOTO[†a)], *Member*

SUMMARY A stacked rectangular microstrip antenna with a shorting plate and a helical pin is proposed as a car antenna for triple band operation in ITS. The proposed antenna operates as a conventional stacked microstrip antenna at the highest frequency band. At the middle and the lowest frequency bands, the antenna radiates at low elevation angles from the helical pin and the shorting plate. In this paper, as an example of triple band antennas in the ITS, an antenna is designed that supports PHS, VICS and ETC. The proposed antennas have the proper radiation pattern for each application and are small in size.

key words: stacked microstrip antenna, triple band operation, helical pin, shorting plate, ITS (Intelligent Transport Systems)

1. Introduction

ITS (Intelligent Transport Systems) has received much attention as a system for traffic safety and environmental protection. ITS applications such as ETC (electric toll collection system), GPS (global positioning system), SDRAS (satellite digital audio radio service) and VICS (vehicle information and communications system) are proposed and widely used presently. In the future, ITS will be developed as a system for ubiquitous communication, too. Next generation PHS (personal handy phone system), Cellular phone and Mobile Wimax (worldwide interoperability for microwave access) are candidates for ubiquitous communication. In order to use all these applications, multi band antennas represent an effective solution as car antennas for the ITS.

So far, many single feed microstrip antennas (MSAs) for multi band operation have been proposed [1]–[6]. However, most of them are antennas with linear polarization in two or three frequency bands for mobile phones and wireless LAN applications. In the ETC, GPS and SDARS, a circularly polarized wave is used. While a linearly polarized wave is used in the VICS. Therefore, car antennas have to radiate both the circularly polarized wave and the linearly polarized wave. The design of single feed MSAs for three or more frequency operation for ITS is difficult compared to those with only linear polarization.

The author has proposed stacked MSA with a shorting plate as a car antenna for VICS and ETC [7]. In the higher frequency band, the proposed antenna operates as a

conventional half-wavelength stacked MSA with a perturbation segment. Therefore, the proposed antenna radiates a circularly polarized wave at high elevation angles where the toll gate antennas are installed. In the lower frequency band, since the electric current flows strongly on the shorting plate, the peak of the radiation field is at low elevation angles. Therefore, the antenna receives signals with uniform level within the communication area for the VICS [7]–[9].

In this paper, a stacked rectangular MSA with a shorting plate and a helical pin is proposed as a car antenna for triple band operation in ITS. The conventional helical antenna offers normal and axial modes [10]. In the proposed antenna, the normal mode is used. The normal mode has a radiation pattern suitable for mobile communications and the antenna is low profile. MSAs loading a helical pin haven't been studied, yet. The relationships between a new resonant mode produced by the helical pin and the other resonant modes by the shorting plate and the stacked rectangular patches are clarified by numerical simulation. In order to present the validity of the proposed antenna, the proposed antenna is designed for PHS as used at present, VICS and ETC operation. To the author's knowledge, no antennas for triple band operation with the proper radiation pattern for each application in the ITS have been proposed.

For the calculations in this paper, the simulation software package IE3D 10.2, which is based on the method of moments in the spectral domain (SD-MoM), is used [11]. In the SD-MoM, Green's functions for layered mediums are used [12]. Therefore, the simulator IE3D is efficient for analyzing stacked MSAs. In order to ascertain the accuracy of the calculated results, the calculated return loss, axial ratio and radiation pattern are compared with experimental data.

2. Antenna Design

Figures 1(a) and (b) show perspective and side views of a stacked rectangular MSA with a shorting plate and a helical pin, respectively. The antenna consists of a dielectric substrate and a layer of air with a rectangular patch. The upper and lower patches are the same size and their widths and lengths are W and L. The upper patch is shorted to the lower patch at the apex by a conducting plate. The width of the shorting plates is d_S. A helical pin is loaded on the lower patch at the point x_h, y_h. The center of the helical pin in xy plane is at x_s, y_s. The number and the diameter of turns of the helical pin are N and C_h, respectively. The diameter and the height of the helical pin is $C_w=1.0$ mm and h_3, re-
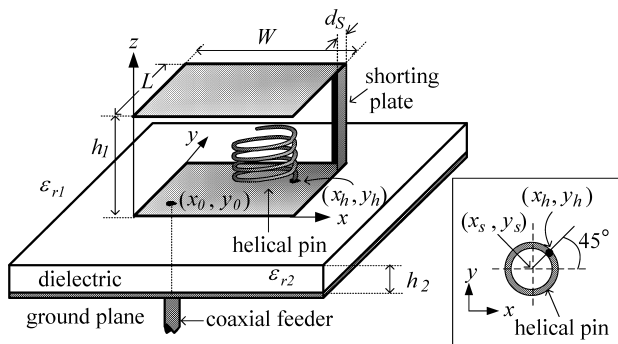
(a) perspective view
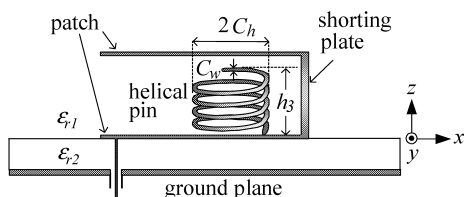
(b) side view

Fig. 1 Geometry of stacked rectangular microstrip antenna with a shorting plate and a helical pin and its coordinate system.

Fig. 2 Calculated input impedances (W=12.9 mm, L=16.1 mm, h_1=9.6 mm, h_3=6.0 mm, d_S=1.5 mm, C_h=3.0 mm, N=2.5, x_s=8.0 mm, y_s=10.0 mm, x_0=3.0 mm, y_0=3.8 mm).

spectively. The relative dielectric constant and the thickness of the upper and lower layers are ε_{r1}=1.0, h_1 and ε_{r2}=2.6, h_2=2.4 mm, respectively. The antenna is excited at the lower patch by a coaxial feed through the lower dielectric substrate at point x_0, y_0 which lays around the diagonal.

3. Three Resonant Modes

Figure 2 shows the input impedance calculated by the simulator IE3D in the antennas with and without a helical pin. In the calculation by the simulator IE3D, the size of the ground plane is infinite. The antenna without a helical pin has two resonant modes [7]. In the proposed antenna, however, a new resonant mode is produced by loading a helical pin around 2.6 GHz.

Figures 3(a) and (b) show time averaged electric current distributions at resonant frequencies in the lowest and middle bands. Figure 3(c) shows time averaged electric current distribution at frequency giving the best axial ratio in the highest band. The electric current distributions of antenna with a helical pin at the highest and lowest bands are similar to those without a helical pin at two frequency bands [7]. At the highest frequency band, the width and length of the patches approximately become a half wavelength and the intensity of the electric current on the upper patch is much smaller than that on the lower patch. These characteristics of the electric current denote that the antenna operates as the conventional half–wavelength stacked MSA with a perturbation segment. Therefore, the proposed antenna radiates a circularly polarized wave with the appropriate ratio (L/W) of the length to the width of the rectangular patch conductor.
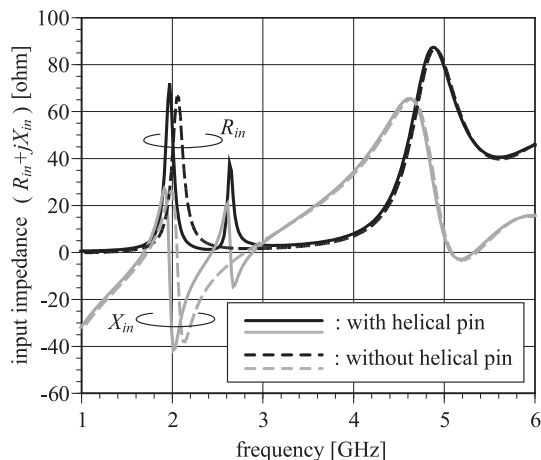
At the lowest frequency band, the antenna resonates when the sum of the lengths of the diagonal of the upper and lower patches and the shorting plate becomes a half wavelength. Since the intensity of the electric current on the shorting plate is the biggest, the antenna radiates strongly from the shorting plate. Therefore, the antenna doesn't operate as the conventional stacked MSA but as a single antenna element. It is observed that electric currents are excited on the helical pin. They are induced on the helical pin by the electric currents with greater intensity on the shorting plate. At the middle frequency band, the electric current flows strongly on the helical pin, that is, the helical pin operates as the radiation element. In this paper, the resonant mode of the conventional stacked MSA is referred to as P-mode, the resonant mode by the shorting plate is referred to as S-mode and the resonant mode by the helical pin is referred to as H-mode.

Figures 4(a)–(c) show the calculated radiation patterns on xz and yz planes at the S-mode, the H-mode and the P-mode, respectively. Since the size of the ground plane is infinite in the calculation by the simulator IE3D, the antenna doesn't radiate behind the ground plane. Moreover, the radiation pattern around z=0 cannot be calculated accurately. Therefore, the calculated radiation patterns are shown for the angles $0° \leq \theta \leq 85°$. At the S-mode, the radiation peak is at low elevation angles. This is due to the fact that the radiation fields by the electric currents on the upper and lower patches (flowing to the opposite directions) cancel out each other around high elevation angles and the maximum radiation fields due to the electric current on the vertical shorting plate are in the broadside direction [7]. At the H-mode, the radiation peak is at low elevation angels, which is similar to the case of the S-mode. These radiation patterns at the H-mode denote that the proposed antenna operates as the normal mode in a conventional helical antenna with ground plane [10]. At the P-mode, the antenna radiates at high elevation angles as a conventional stacked MSA.
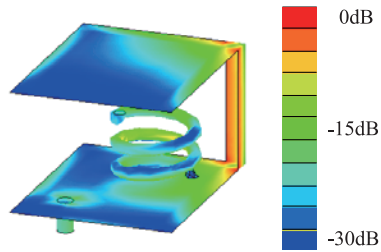
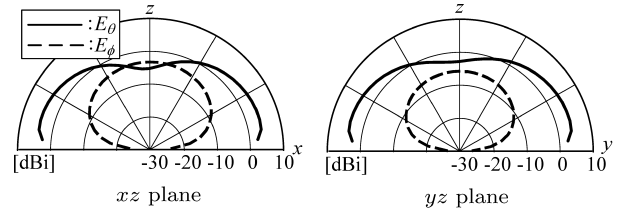(a) At the lowest frequency band (frequency=1.96 GHz)
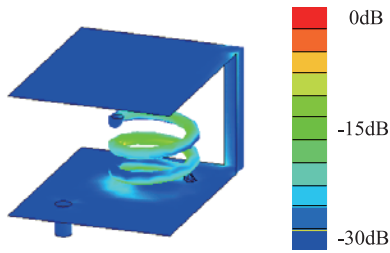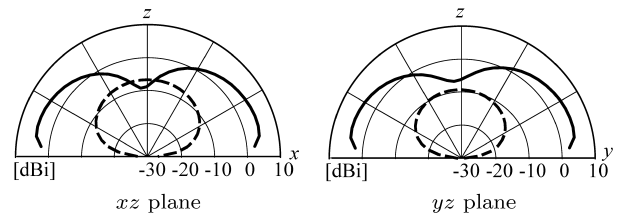

(b) At the middle frequency band (frequency=2.64 GHz)
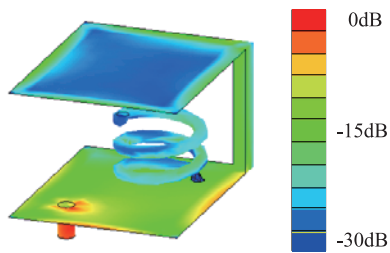
(c) At the highest frequency band (frequency=5.70 GHz)

Fig. 3 Time averaged electric current distributions at three frequency bands (W=12.9 mm, L=16.1 mm, h_1=9.6 mm, h_3=6.0 mm, d_S=1.5 mm, C_h=3.0 mm, N=2.5, x_s=8.0 mm, y_s=10.0 mm, x_0=3.0 mm, y_0=3.8 mm).

(a) At the lowest frequency band (S-mode, frequency=1.96 GHz)

(b) At the middle frequency band (H-mode, frequency=2.64 GHz)

(c) At the highest frequency band (P-mode, frequency=5.70 GHz)

Fig. 4 Calculated radiation patterns at three frequency bands (at three resonant modes) (W=12.9 mm, L=16.1 mm, h_1=9.6 mm, h_3=6.0 mm, d_S=1.5 mm, C_h=3.0 mm, N=2.5, x_s=8.0 mm, y_s=10.0 mm, x_0=3.0 mm, y_0=3.8 mm).
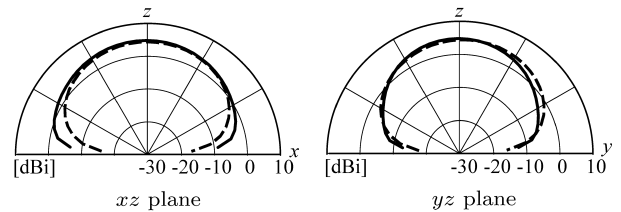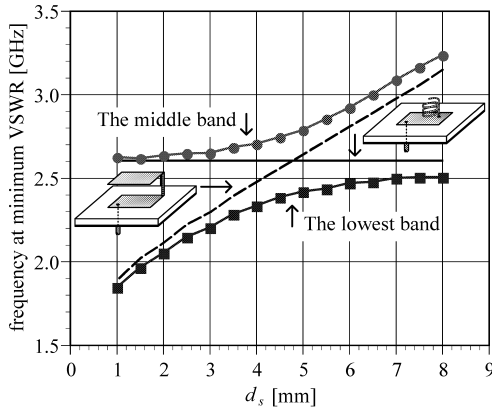
Figure 5(a) shows the frequencies giving the minimum VSWR at the lowest and middle frequency bands for change of the width of the shorting plates d_S. Those of the antenna without a helical pin and those of the antenna without an upper patch and a shorting plate are also shown for comparison. The locations of the feed point in all antennas are fixed. As the width of the shorting plate increases, the frequencies at the lowest and middle bands increase. These frequencies can be controlled in a wide range by adjusting the width of the shorting plate. The frequencies of the two antennas calculated for comparison serve as asymptotes to the frequencies at the lowest and middle bands. The proposed antenna is divided into three types by the relationship between the modes and the frequencies at the lowest and middle bands. In the first type, the frequency at the middle band is close to the asymptote of the antenna without an upper patch and a shorting plate and the frequency at the lowest band is close to the asymptote of the antenna with-

out a helical pin at the narrow width d_S. These denote that the frequency at the middle band is the frequency of the H-mode and the frequency at the lowest band is the frequency of the S-mode. The characteristics of the second type are opposite to those of the first type. This type appears at the wide width d_S. In the third type, the modes of two bands are undefined around the area where two asymptotes cross. From the viewpoint of antenna miniaturization, the use of a narrow width d_S is an effective solution.
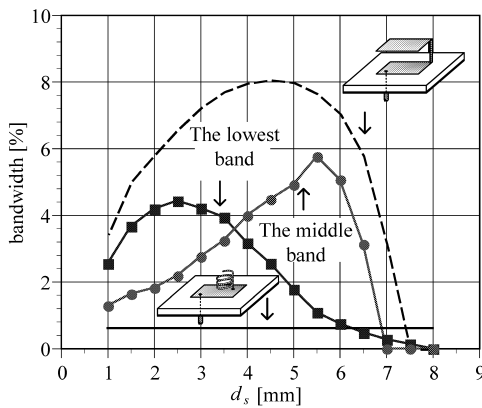
Figure 5(b) shows the bandwidth (VSWR ≤ 2) at the lowest and middle frequency bands for change of the width of the shorting plates d_S. Since the impedance matching isn't tuned at $d_S ≥ 7.0$ mm, the bandwidths of the H-mode and the S-mode are approximately 0. At $d_S ≤ 6.0$ mm, the bandwidth of the proposed antenna is greater than that of the antenna without an upper patch and a shorting plate. On the contrary, the bandwidth of the S-mode becomes narrow compared to that of the antenna without a helical pin.

Figure 6 shows the frequency giving the best axial ratio and the bandwidth (VSWR ≤ 2 with axial ratio ≤ 3 dB) at the highest frequency band. The frequency at the highest band is constant and the change of the bandwidth is small for change of d_S. Since the proposed antenna operates as the conventional stacked MSA at the highest frequency band,

the bandwidth is wide. According to calculations, the best axial ratio is less than 0.52 dB at 1.0 mm $\leq d_S \leq$ 8.0 mm, but is omitted in this paper. The effect of the width d_S on the high frequency band is very small.

4. Parameter Study of Helical Pin

As mentioned in the previous section, the antenna size can be reduced as the width d_S decreases. Therefore, the antenna with the width $d_S =$ 3.0 mm is discussed in this section.

Figure 7(a) shows the frequencies f_S and f_H giving the minimum VSWR at the S-mode and the H-mode for change

(a) Frequencies at the minimum VSWR

(b) Bandwidths

Fig. 5 Frequencies at minimum VSWR and bandwidth at the lowest and middle frequency bands for change of d_S. (W=12.9 mm, L=16.1 mm, h_1=9.6 mm, h_3=6.0 mm, C_h=3.0 mm, N=2.5, x_s=8.0 mm, y_s=10.0 mm, x_0=3.0 mm, y_0=3.8 mm).
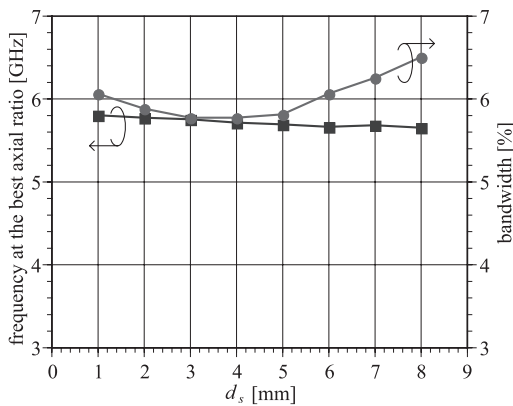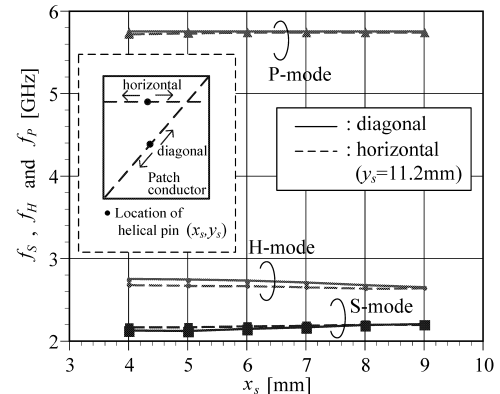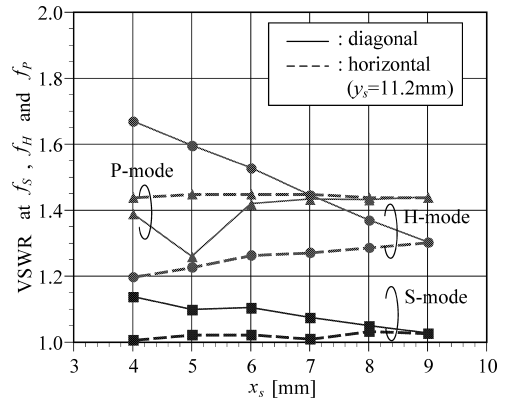

Fig. 6 Frequency at the best axial ratio and bandwidth at the highest frequency band for change of d_S (W=12.9 mm, L=16.1 mm, h_1=9.6 mm, h_3=6.0 mm, C_h=3.0 mm, N=2.5, x_s=8.0 mm, y_s=10.0 mm, x_0=3.0 mm, y_0=3.8 mm).

(a) Frequencies f_S, f_H and f_P

(b) VSWR at f_S, f_H and f_P
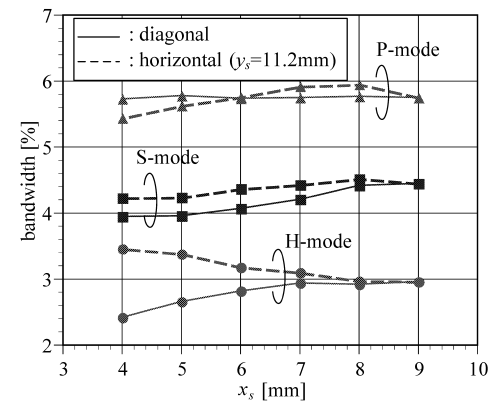
(c) Bandwidth

Fig. 7 Frequencies (f_S, f_H and f_P) VSWR and bandwidth at three modes for change of x_s. (W=12.9 mm, L=16.1 mm, h_1=9.6 mm, h_3=6.0 mm, d_S=3.0 mm, C_h=3.0 mm, N=2.5, x_0=3.0 mm, y_0=3.8 mm).

of the location of the helical pin. Figure 7(a) also shows the frequency f_P giving the best axial ratio at the P-mode. Figures 7(b) and (c) show the VSWR at frequencies f_S, f_H and f_P and the bandwidths of all modes, respectively. The feed point is fixed. The location of the helical pin doesn't affect the frequencies at all modes (Fig. 7(a)). The influences of the location of the helical pin on the VSWRs and bandwidths at the S-mode and the P-mode are very small (Figs. 7(b) and (c)). According to calculations, moreover, the changes of the best axial ratio at the P-mode is from 0.38 dB to 0.69 dB (but is omitted in this paper). As shown in Fig. 7(b), however, the VSWR of the H-mode varies widely. It is generally difficult to tune impedance matching at three frequency bands. In the proposed antenna, however, the impedance matching of the S-mode and the P-mode can be tuned by the location of the feed point and that of the H-mode can be tuned by the location of the helical pin. As shown in Fig. 7(b), the VSWR of the H-mode with change of the location along the horizontal is 1.3 or less. In spite of sufficiently small VSWR, the bandwidth of the H-mode varies approximately from 2.9% to 3.5%. This is due to the change of the mutual coupling between the shorting plate and the helical pin and this denotes that the bandwidth of the H-mode can be adjusted by changing the location of the helical pin.

Figure 8(a) shows the frequencies giving the minimum VSWR at the lowest and middle frequency bands as the radius of the helical pin C_h changes. These frequencies at two bands can be controlled in a wide range by changing the radius C_h. This result depending on the radius C_h is the same characteristic as the case of the width d_S shown in Fig. 5(a). Figure 8(b) shows the bandwidth for change of the radius of the helical pin C_h. The bandwidth of the antenna without a helical pin is also shown for comparison. As the thickness h_1 increases, the bandwidths in the lowest frequency band at $C_h \leq 3.0$ mm and in the middle frequency band at $C_h \geq 3.4$ mm, which are the frequency bands of the S-mode, increase. This is due to the following reason. As the thickness h_1 increases, the Quality factor Q of the upper patch decreases. Therefore, the bandwidth of the S-mode increases [7].

Figure 9 shows the frequency giving the best axial ratio and the bandwidth at the highest band for change of the radius of the helical pin C_h. The radius C_h doesn't affect the frequency at the highest band. The bandwidth is constant except at the radius $C_h = 3.2$ mm. This is due to the fact that the higher mode of the H-mode occurs around the highest frequency band at the radius $C_h = 3.2$ mm. According to calculations, the best axial ratios are less than 0.6 dB at 2.2 mm $\leq C_h \leq 3.8$ mm.

The case in which the width $d_S = 1.0$ mm is also simulated but the results are omitted in this paper. They are similar to those in which the width $d_S = 3.0$ mm shown in Figs. 7, 8 and 9.

Similarly, the parameters of the height and the number of the helical pin, h_3 and N, have been studied. As the height h_3 increases, the both frequencies at the lowest and
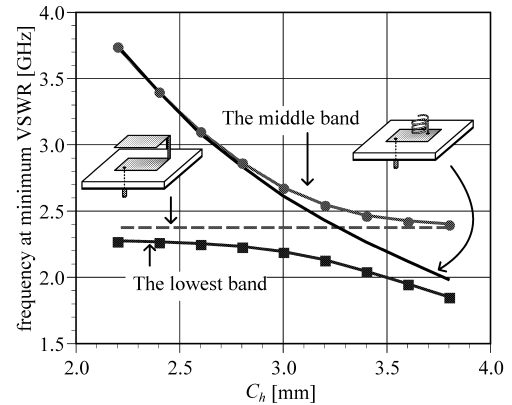
(a) Frequencies at minimum VSWR (h_1=9.6 mm)
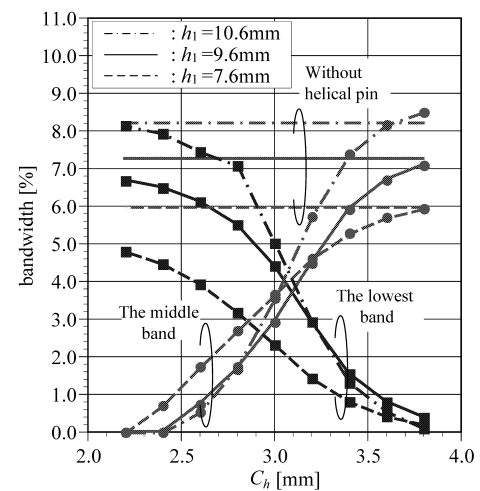
(b) Bandwidth

Fig. 8 Frequencies and bandwidths at the lowest and middle frequency bands for change of C_h (W=12.9 mm, L=16.1 mm, h_3=6.0 mm, d_S=3.0 mm, N=2.5, x_s=8.0 mm, y_s=10.0 mm, x_0=3.0 mm, y_0=3.8 mm).

middle bands increase and as the number N decreases, the both frequencies increase. The height h_3 and the number N don't influence the characteristics at the P-mode (the highest frequency band) as observed in the case for change of the radius C_h shown in Fig. 9. Therefore, the frequencies, axial ratio and the bandwidth at the P-mode can be tuned by the shorting plate and the patch conductor regardless of the helical pin.

Design procedure for triple band frequency can be obtained by the parameter study mentioned above. At first, the size of the rectangular patch is adjusted to tune the frequency f_P and the axial ratio at the P-mode and after that the width d_S of the shorting plate, the radius, the number of the turns or the height of the helical pin are adjusted to tune the frequencies f_S and f_H at the S-mode and the H-mode. At last, the feed point is adjusted to tune the impedance matching at the P-mode and the S-mode and the location of the helical pin is adjusted to tune the impedance matching at the H-mode.
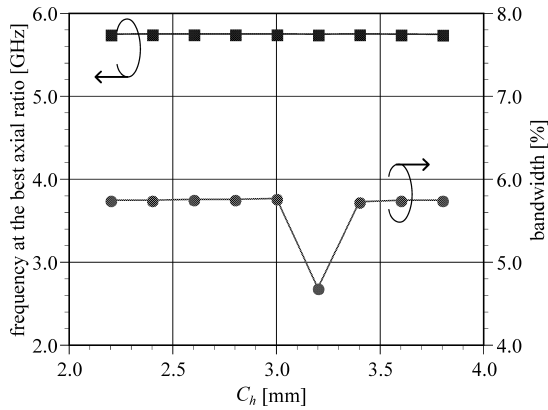
Fig. 9 Frequency at the best axial ratio and bandwidths at the highest frequency band for change of C_h (W=12.9 mm, L=16.1 mm, h_1=9.6 mm, h_3=6.0 mm, d_S=3.0 mm, N=2.5, x_s=8.0 mm, y_s=10.0 mm, x_0=3.0 mm, y_0=3.8 mm).

## 5. Design of Triple Band Antenna for ITS

In order to show validity of the proposed antenna, in this section, the proposed antenna is designed using the design procedure stated in the previous section for the PHS, VICS and ETC. In order to miniaturize the antenna size, the width d_S is designed as narrow as possible. Therefore, the width d_S is set to 1.3 mm. The PHS is chosen as an example of the applications in the ubiquitous communication. Table 1 shows the specifications of the PHS, VICS and ETC.

The communication area for the VICS extends 35 m in both directions from the beacon antenna installed at the shoulder of the road. In such a case, the radiation peak of the car antenna must be at low elevation angles along the road [7]–[9]. The communication area for the ETC is very narrow (the extent is 4 m in one direction from the toll gate antenna) and the toll gate antennas are installed above the car antenna [7]. Therefore, it is desirable that the car antenna for the ETC has a radiation peak at high elevation angles. Since the communication for the PHS is very wide, the radiation pattern of the monopole antenna type is required. The center frequency f_0 and the bandwidth of the VICS in Japan are 2.4997 GHz and 85 kHz and those in the PHS are 1.9 GHz and 35 MHz. In order to keep high communication quality for a mobile communication system with a wide area such as VICS and PHS, it is desirable for the bandwidth to be as wide as possible. In this paper, therefore, a bandwidth of 50 MHz is aimed for in the both VICS and PHS bands. The center frequency f_0 and the bandwidth of the ETC are 5.8 GHz and 100 MHz. Linear polarization is used for the PHS and VICS while circular polarization is used for the ETC.

Figures 10 and 11 show the measured and calculated VSWRs and the axial ratios, respectively. The antenna was made of copper-clad Glass-fiber-PTFE. The dimension of the dielectric substrate of the prototype is 150 mm×150 mm=0.95$\lambda_{1.9}$×0.95$\lambda_{1.9}$=1.25$\lambda_{2.5}$×1.25$\lambda_{2.5}$=2.9$\lambda_{5.8}$×2.9$\lambda_{5.8}$ (λ_f: the wave length at f GHz). The

Table 1 Specification of PHS, VICS and ETC.

	PHS	VICS	ETC
frequency f_0 [GHz]	1.9	2.5	5.8
Bandwidth [MHz]	50	50	100
Bandwidth [%]	2.63	2.0	1.73
Polarization	Linear	Linear	Circular
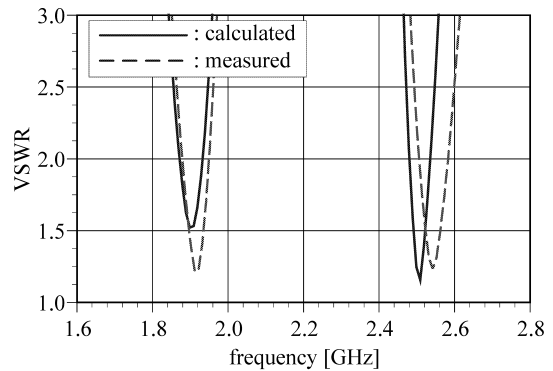
(a) At the lowest and the middle frequency bands
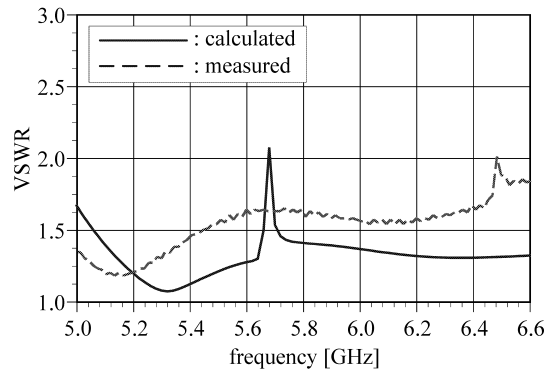
(b) At the highest frequency band

Fig. 10 Calculated and measured VSWRs (W=12.9 mm, L=16.1 mm, h_1=9.6 mm, h_3=6.5 mm, d_S=1.3 mm, C_h=3.2 mm, N=2.5, x_s=8.5 mm, y_s=10.6 mm, x_0=3.0 mm, y_0=3.8 mm).
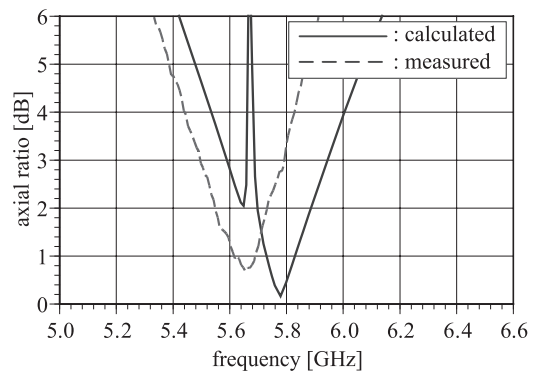

Fig. 11 Calculated and measured axial ratios (W=12.9 mm, L=16.1 mm, h_1=9.6 mm, h_3=6.5 mm, d_S=1.3 mm, C_h=3.2 mm, N=2.5, x_s=8.5 mm, y_s=10.6 mm, x_0=3.0 mm, y_0=3.8 mm).

(a) At the lowest resonant frequency (calculated:1.9 GHz, measured:1.91 GHz)

(b) At the middle resonant frequency (calculated:2.5 GHz, measured:2.52 GHz)

(c) At the highest resonant frequency (calculated:5.78 GHz, measured:5.66 GHz)
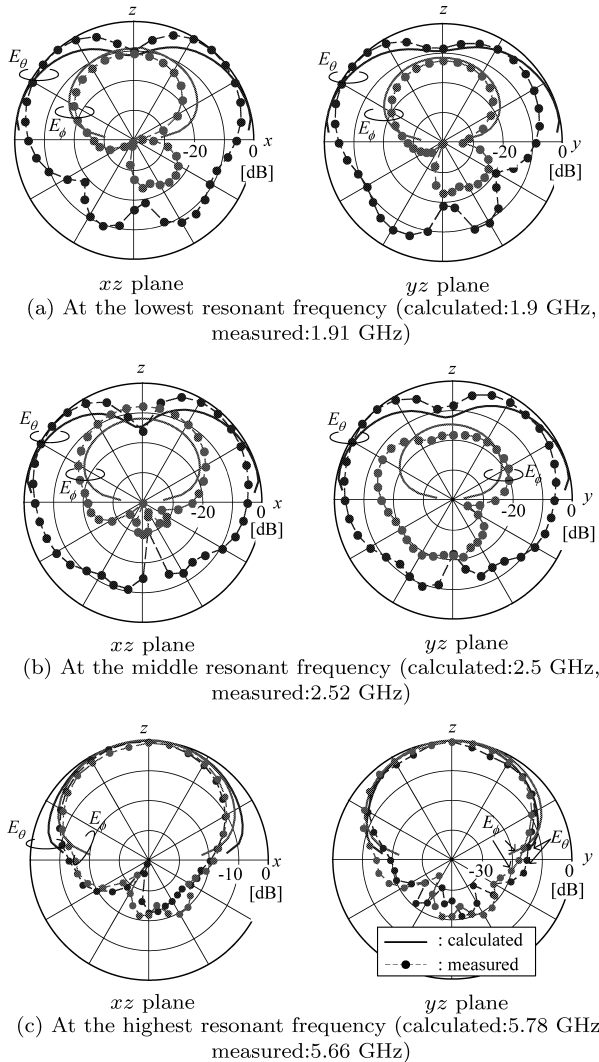
Fig. 12 Calculated and measured radiation patterns at three resonant frequencies (W=12.9 mm, L=16.1 mm, h_1=9.6 mm, h_3=6.5 mm, d_S=1.3 mm, C_h=3.2 mm, N=2.5, x_s=8.5 mm, y_s=10.6 mm, x_0=3.0 mm, y_0=3.8 mm).

measured bandwidths (VSWR ≤ 2) in the PHS and VICS bands are 73 MHz (3.81%) and 77 MHz (3.03%), respectively. The measured bandwidth (VSWR ≤ 2 with axial ratio ≤ 3 dB) in the ETC band is 295 MHz (5.23%). The designed antenna satisfies the specification of the bandwidths in the triple bands. The relative errors of the center frequency between the calculated and measured results in the PHS, VICS and ETC bands are 0.71%, 1.66% and 2.74 %, respectively. The measured center frequencies agree well with the calculated ones. The calculated VSWR and axial ratio have the singularity around 5.66 GHz in the ETC band and the measured ones have the singularity around 6.5 GHz. The difference between the measured and calculated frequencies giving the singularity due to the higher mode of the H-mode is very big. This is due to the fact that the production error of the prototype for the wavelength at the higher mode becomes big compared with that at the primary mode which is excited around 2.5 GHz.

Table 2 Calculated and measured gains in xz plane or yz plane (W=12.9 mm, L=16.1 mm, h_1=9.6 mm, h_3=6.5 mm, d_S=1.3 mm, C_h= 3.2 mm, N=2.5, x_s=8.5 mm, y_s=10.6 mm, x_0=3.0 mm, y_0=3.8 mm).

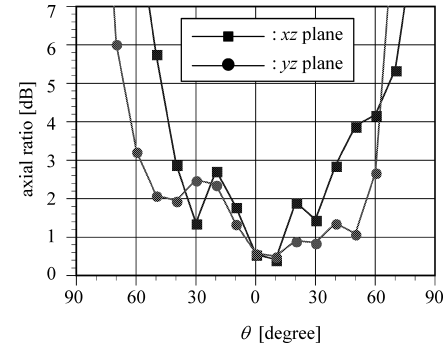|	PHS	VICS	ETC
calculated gain [dBi]	3.32	3.40	6.09
measured gain [dBi]	2.50	2.40	6.08

Fig. 13 Measured axial ratios in xz plane and yz plane (W=12.9 mm, L=16.1 mm, h_1=9.6 mm, h_3=6.5 mm, d_S=1.3 mm, C_h=3.2 mm, N=2.5, x_s=8.5 mm, y_s=10.6 mm, x_0=3.0 mm, y_0=3.8 mm).

Figures 12(a)–(c) show the measured and calculated radiation patterns normalized by the maximum value of the electric fields in the xz and yz planes. Table 2 shows the maximum gain in either xz plane or yz plane. In the PHS and VICS bands, the differences between the calculated and measured radiation patterns are due to the edge diffractions of the finite ground plane [7], [9]. Moreover, the measured gains are approximately 1.0 dBi less than the calculated ones in the PHS and VICS bands. This is due to the fact that the antenna radiates greatly behind the ground plane because the size of the ground plane of the prototype for the wavelength is very small ($0.95\lambda_{1.9}\times0.95\lambda_{1.9}$, $1.25\lambda_{2.5}\times1.25\lambda_{2.5}$). In the ETC band, however, the size of the finite ground plane is large compared with the wavelength ($2.9\lambda_{5.8}\times2.9\lambda_{5.8}$). Therefore, the calculated radiation patterns and maximum gain agree well with the measured ones. In the PHS and VICS bands, the radiation peak is at low elevation angles. In the ETC band, the radiation peak is at high elevation angles. These radiation patterns are the characteristics required for a car antenna for the PHS, VICS and ETC.

The radiation angle of circularly polarized wave is very important in the ETC. Figure 13 shows the measured radiation angles of circularly polarized wave in xz plane and yz plane. The angles with the axial ratio ≤ 3 dB are approximately 80 degrees in xz plane and 120 degrees in yz plane. The proposed antenna radiates circularly polarized wave at wide angles.

In the designed antenna, the averaged width and length $(W+L)/2$ is equal to 14.5 mm=$0.092\lambda_{1.9}$=$0.12\lambda_{2.5}$=$0.28\lambda_{5.8}$ (λ_f : the wave length at f GHz). The height (h_1+h_2) of the antenna is equal to 12.0 mm=$0.076\lambda_{1.9}$=$0.10\lambda_{2.5}$=$0.23\lambda_{5.8}$. The designed antenna is small in size.

6. Conclusion

A stacked rectangular MSA for triple band operation has been proposed and an antenna for PHS, VICS and ETC applications in ITS has been designed. The three resonant modes are achieved by shorting the upper patch to the lower patch at an apex and by loading a helical pin on the lower patch conductor.

The operational principles of the antenna were discussed using the electric current distributions and the radiation patterns. In the highest frequency band, the proposed antenna operates as a conventional half-wavelength stacked MSA with a perturbation segment. Therefore, the antenna radiates a circularly polarized wave at high elevation angles. In the lowest and middle frequency bands, a linearly polarized wave is radiated to low elevation angles from the shorting plate and the helical pin, or from the both elements at the same time. Main radiation elements at the lowest and middle frequency bands depend on the width of the shorting plate and the geometrical parameters of the helical pin.

Moreover, the relationships between antenna characteristics at three operational frequencies and the geometrical parameters of the antenna have been investigated. The lowest and middle frequencies can be controlled in a wide range by adjusting the width of the shorting plates or the geometrical parameters of the helical pin. A resonant mode by the helical pin is the normal mode in a conventional helical antenna with ground plane. Although the bandwidth of the normal mode is very narrow, the bandwidth by the helical pin in the proposed antenna is improved by the mutual effect between the helical pin and the shorting plate. The influences of the helical pin and the shorting plate on the highest frequency band operated by the stacked patches are very small. Moreover, the impedance matching of the three frequencies can be tuned by the location of the feed point and the location of the helical pin. These denote that the proposed antenna is useful for designing the triple band antenna.

The proposed antenna is small and has suitable radiation patterns for the VICS and ETC in the ITS and ubiquitous communication applications. In this paper, although the PHS used at present is chosen as an application of the ubiquitous communication, the proposed antenna can be applied to Next generation PHS, Cellular phone and Mobile Wimax.

Acknowledgments

References

[1] K.L. Wong, "Compact dual–frequency and dual–polarized microstrip antennas," in Compact and Broadband Microstrip Antennas, ed. K. Chang, pp.87–161, John Wiley & Sons, New York, 2002.

[2] K.L. Wong, "Broadband dual–frequency and dual–polarized microstrip antennas," in Compact and Broadband Microstrip Antennas, ed. K. Chang, pp.279–293, John Wiley & Sons, New York, 2002.

[3] Y.X. Guo, K.M. Luk, and K.F. Lee, "A quarter-wave U-shaped patch antenna with two unequal arms for wideband and dual–frequency operation," IEEE Trans. Antennas Propag., vol.50, no.8, pp.1082–1087, Aug. 2002.

[4] J.H. Lu, "Broadband dual–frequency operation of circular patch antennas and arrays with a pair of L–shaped slots," IEEE Trans. Antennas Propag., vol.51, no.5, pp.1018–1023, May 2003.

[5] K.L. Lau, K.C. Kong, and K.M. Luk, "A miniature folded shorted patch antenna for dual-band operation," IEEE Trans. Antennas Propag., vol.55, no.8, pp.2391–2398, Aug. 2007.

[6] S.J. Lin and J.S. Row, "Monopolar patch antenna with dual–band and wideband operations," IEEE Trans. Antennas Propag., vol.56, no.3, pp.900–903, March 2008.

[7] T. Fujimoto and K. Tanaka, "Stacked rectangular microstrip antenna with a shorting plate for dual band (VICS/ETC) operation in ITS," IEICE Trans. Commun., vol.E90-B, no.11, pp.3307–3310, Nov. 2007.

[8] Y. Kazama, N. Morita, and S. Tokumaru, "Mobile communications higher–order–mode microstrip antennas for road vehicle communications," IEICE Trans. Commun. (Japanese Edition), vol.J82-B, no.10, pp.1898–1904, Oct. 1999.

[9] T. Fujimoto, S. Noguchi, K. Tanaka, and M. Taguchi, "Stacked square microstrip antenna with a shorting post for road vehicle communication," RF and Microwave Computer-Aided Engineering, vol.14, no.3, pp.244–252, May 2004.

[10] C.A. Balanis, "Traveling wave and broadband antennas," in Antenna Theory Analysis and Design, 2nd ed., pp.488–540, John Wiley & Sons, 1997.

[11] "IE3D User's Manual," Zeland Software, Dec. 1999.

[12] J.R. Mosig, "Integral equation technique," in Numerical Techniques for Microwave and Millimeter–Wave Passive Structures, ed. T. Itoh, pp.133–213, John Wiley & Sons, New York, 1989.

Takafumi Fujimoto received the B.E and M.E. degrees from Nagasaki University in 1992 and 1994, respectively, and a Dr.Eng. degree from Kyushu University in 2003. He is currently a Associate Professor at Nagasaki University. From Nov. 2004 to Sep. 2005, he was a Visiting Scholar in the department of Electrical and Computer Engineering, University of ILLINOIS at Urbana-Champaign. His main interests are the analytical methods of microstrip antennas, the designing of microstrip antennas in antenna engineering and the diffraction-free beams in optical engineering. Dr. Fujimoto is a member of the IEEE and Optical Society of America (OSA).